Mon. Not. R. Astron. Soc. **392,** 982–991 (2009) doi:10.1111/j.1365-2966.2008.14080.x

The mid-infrared colour–magnitude relation of early-type galaxies in the Coma cluster as measured by *Spitzer*-IRS⋆

M. S. Clemens,[1]† A. Bressan,[1,2,3] P. Panuzzo,[4] R. Rampazzo,[1] L. Silva,[5] L. Buson[1] and G. L. Granato[5]

[1]*INAF–Osservatorio Astronomico di Padova, Vicolo dell'Osservatorio, 5, 35122 Padova, Italy*
[2]*SISSA–ISAS, International School for Advanced Studies, ia Beirut 4, 34014 Trieste, Italy*
[3]*INAOE, Luis Enrique Erro 1, 72840, Tonantzintla, Puebla, Mexico*
[4]*Laboratoire AIM, CEA/DSM – CNRS – Université Paris Diderot, DAPNIA/Service d'Astrophysique, Bât. 709, CEA-Saclay, F-91191 Gif-sur-Yvette Cédex, France*
[5]*INAF, Osservatorio Astronomico di Trieste, Via Tiepolo 11, I-34131 Trieste, Italy*

Accepted 2008 October 13. Received 2008 October 13; in original form 2008 August 12

ABSTRACT

We use 16 μm, *Spitzer*-Infrared Spectrograph, blue peak-up photometry of 50 early-type galaxies in the Coma cluster to define the mid-infrared colour–magnitude relation. We compare with recent simple stellar population models that include the mid-infrared emission from the extended, dusty envelopes of evolved stars. The K_s-[16] colour in these models is very sensitive to the relative population of dusty asymptotic giant branch stars. We find that the *passively evolving* early-type galaxies define a sequence of approximately constant age (∼10 Gyr) with varying metallicity. Several galaxies that lie on the optical/near-infrared colour–magnitude relation do not lie on the mid-infrared relation. This illustrates the sensitivity of the K_s-[16] colour to age. The fact that a colour–magnitude relation is seen in the mid-infrared underlines the extremely passive nature of the majority (68 per cent) of early-type galaxies in the Coma cluster. The corollary of this is that 32 per cent of the early-type galaxies in our sample are *not* 'passive', insofar as they are either significantly younger than 10 Gyr or they have had some rejuvenation episode within the last few Gyr.

Key words: galaxies: clusters: general – galaxies: elliptical and lenticular cD – galaxies: evolution – galaxies: photometry.

1 INTRODUCTION

Early-type galaxies (ETGs; ellipticals and S0s) are ancient stellar populations whose epoch of formation is related to the large-scale structure formation in the Universe. This picture is supported by various studies that have used optical line-strength indices to determine evolutionary parameters of ETGs in the cluster and field environments (see Renzini 2006 for a review). Among these studies, some authors (Bernardi et al. 2005; Thomas et al. 2005; Clemens et al. 2006; Sánchez-Blázquez et al. 2006a; Annibali et al. 2007) suggest that cluster ETGs have a luminosity weighted, mean stellar age 1–2 Gyr older than those in the field. Recently, Trager, Faber & Dressler (2008) challenged this view. Analysing the Coma cluster, they found that the 12 ETGs in their sample have mean single stellar population equivalent ages of 5–8 Gyr, with the oldest systems being ≤10 Gyr old. This average age is remarkably similar to the mean age of ETGs in low-density environments (see e.g. Annibali et al. 2007, and references therein).

The emission from elliptical galaxies longward of ∼10 μm has a large contribution from the circumstellar dust around evolved stars, such as those on the asymptotic giant branch (AGB). This dust emission has been detected by *Spitzer* in ETGs where it is seen as a wide emission feature near 10 μm with another broad feature near 18 μm (Bressan et al. 2006). The spatial profile in the mid-infrared (MIR) is similar to the optical profile (Temi, Brighenti & Mathews 2008; Athey et al. 2002), re-enforcing the notion that the origin is stellar rather than interstellar medium (ISM). This cicumstellar dust has also been detected directly as an extended envelope around nearby AGB stars (Gledhill & Yates 2003). Longer wavelength infrared emission from elliptical galaxies is sometimes detected (Leeuw et al. 2004; Marleau et al. 2006; Temi, Brighenti & Mathews 2007), but this cooler component is probably associated with a diffuse ISM, rather than with evolved stars directly.

For objects older than 0.1 Gyr, the MIR emission traces stars during their mass-losing AGB phase, and this evolutionary phase is

⋆This work is based on observations made with the *Spitzer Space Telescope*, which is operated by the JPL, Caltech under a contract with NASA.
†E-mail: marcel.clemens@oapd.inaf.it

still detected in objects with ages typical of globular clusters such as 47 Tucanae (Lebzelter et al. 2006). Because the luminosity of an AGB star depends on its mass and the main-sequence turn-off mass decreases with time, the MIR emission depends on the age of the stellar population. If all the stars in an ETG were created in an instantaneous burst 10 Gyr ago, the MIR emission would be dominated by stars on the AGB with an initial mass of slightly less than $1\,M_{\odot}$ (for solar metallicity).

The strength of the silicate emission from the dusty envelopes of evolved stars is a function of both age and metallicity. As pointed out by Bressan, Granato & Silva (1998), however, the dependence of this emission on age and metallicity is different to that in the optical.

A colour–magnitude relation which includes a band containing the silicate emission from AGB stars therefore traces the AGB population as a function of the total luminosity, and can, in principle, be used with the optical relation to disentangle the effects of age and metallicity.

Here, we use 16 μm images of 50 ETGs in the Coma cluster, made with the blue peak-up detector of the IRS on *Spitzer*. We combine these with archival *Spitzer* Infrared Array Camera (IRAC) images at 4.5 μm and *K*-band images to construct the MIR colour–magnitude relation. As objects at the distance of the Coma cluster were too faint for IRS spectroscopy, we include four galaxies in the Virgo cluster for which we have IRS spectra. These four objects were selected to have spectra that show no evidence of activity, such as recent star formation or an active galactic nuclei (AGN), and are intended as a 'template' for passive objects against which to compare the more distant objects of Coma.

The Coma cluster is both very rich and dynamically relaxed, and contains some of the most massive galaxies in the local Universe. As such, it is an ideal place to study the star formation history of ETGs.

2 DATA ANALYSIS AND RESULTS

2.1 Mid-infrared photometry

The blue peak-up images (see e.g. Fig. 1) are background dominated, with source fluxes only a few percent above the background level. In addition, the background shows fluctuations on spatial scales of several pixels. This presents a serious problem in the consistent determination of integrated fluxes for sources of different angular sizes. The standard technique of modelling the background as a smoothly varying light distribution, and then subtracting it from the image, tends to overcorrect in the vicinity of larger sources, simply because the source size is similar to that of the background fluctuations. In order to avoid this problem, we have opted to measure colours, rather than integrated fluxes, and to do so within a fixed angular radius of 12 arcsec. The flux within this radius is background

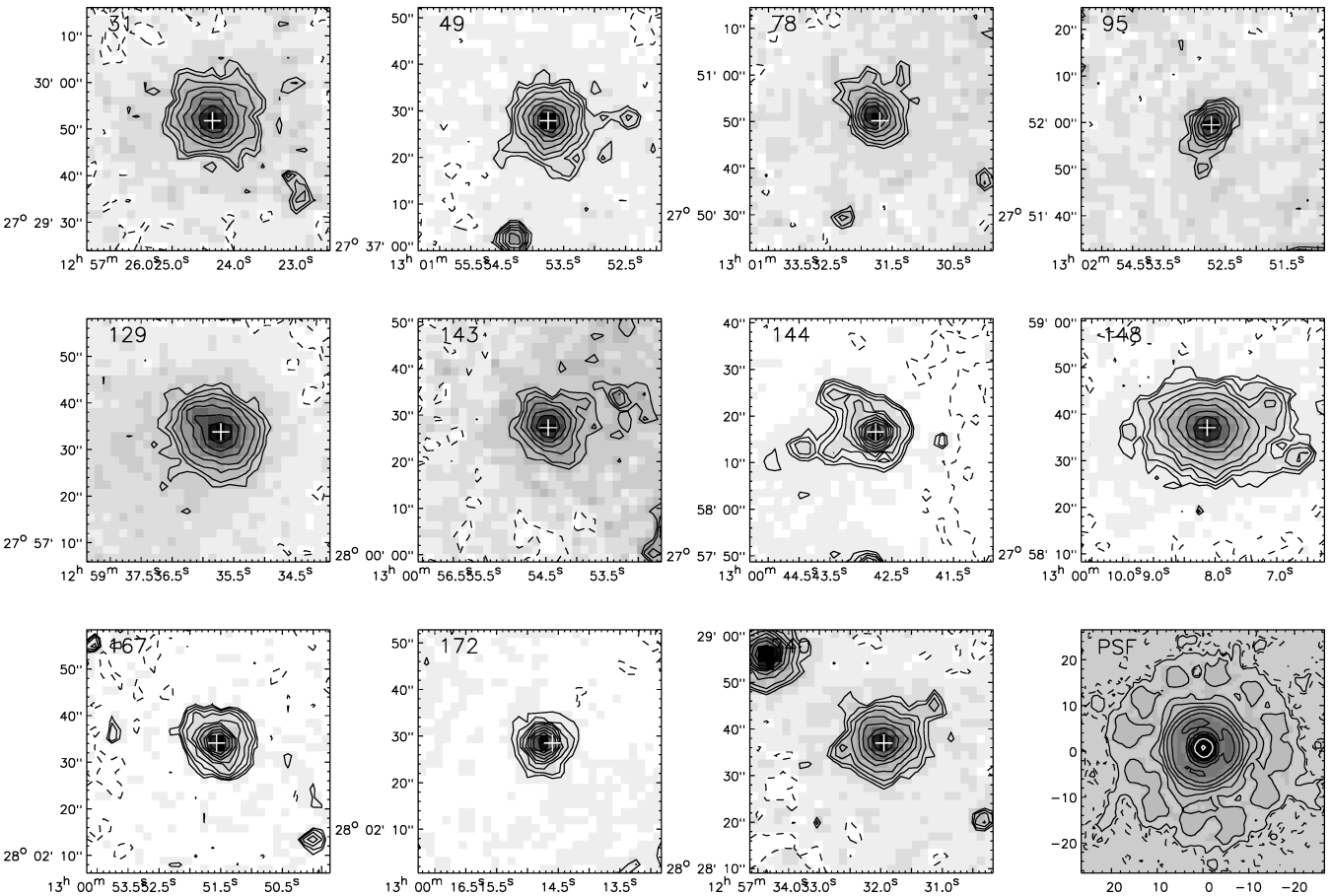

Figure 1. Example background subtracted, Post Basic Calibrated Data, IRS peak-up images of the Coma ETGs. Contour levels are $2^{n/2}/100$, where $n = (-1, 0, 1, 2, \ldots)$ mJy pixel^{-1} with a dashed contour for negative values at the lowest level. The grey-scale in each plot is scaled to the peak source flux. The last panel is an image of the peak-up PSF. The cross in each panel gives the optical source position. The grey-scale has a square-root stretch and contour levels are $2^{n/2}/100$, where $n = (1, 3, 5, \ldots)$ mJy pixel^{-1}. Pixels are 1.8 arcsec on a side.

corrected by subtracting the median pixel value within an annulus just outside this aperture. The error on the derived flux was taken as the quadrature sum of the rms variation within the annulus and the calibration error, which was taken as 5 per cent for the blue peak-up data.

Before applying the same procedure to IRAC channel 2[1] (4.5 μm) and Two-Micron All-Sky Survey (2MASS) K_s-band (2.2 μm) images, these were convolved to the resolution of the IRS peak-up data, in order to remove colour gradients due to the differing instrumental resolutions. The measured aperture fluxes were then used to derive the colours for each object; these colours are presented in Table 1.

Aperture photometry for the four Virgo elliptical galaxies was carried out in an analogous manner, but rather than use a circular aperture of radius 12 arcsec, elliptical apertures of semimajor axis 72 arcsec were used. This difference takes account of the fact that the Virgo cluster is six times closer than Coma cluster and that the images are well resolved. There is a possibility that the use of a larger aperture in the presence of a fixed point spread function (PSF) will introduce a systematic error in the flux determinations between the Coma and Virgo galaxies. In order to verify that this was not a significant source of error, we constructed a number of pairs of simulated galaxy images with de Vaucouleur profiles, differing in their effective radii by a factor of 6. We then convolved each with the IRS blue peak-up PSF and measured the flux within apertures of 12 or 72 arcsec accordingly. The differences in the retrieved fluxes did not exceed 10 per cent, and were typically less than the photometric errors.

All aperture photometry was performed using a custom pipeline written in IDL and use was made of the IDL ASTRONOMY USER'S LIBRARY (Landsman 1995).

2.2 Estimating the effective radii

A direct estimate of the effective radius based on an image with a high background level and fairly low signal-to-noise ratio (S/N) would be rather sensitive to any error in the subtraction of the background level. In order to minimize this problem, rather than finding the radius containing half of the integrated flux, we adopted the following procedure. We first constructed a model galaxy with a de Vaucouleur's $r^{1/4}$ law and convolved it with the IRS blue peak-up PSF. We either assumed that the intrinsic ellipticity of each galaxy at 16 μm was the same as the optical value as given in 'Goldmine'[2] or was circular, where no value was available. After convolution with the PSF, we measured the radial profile in circular apertures and compared this to the same apertures measured on the image. The derived value of the effective radius, R_e, is that of the model galaxy whose PSF-convolved full width at half-maximum (FWHM) was equal to that of the image profile. These values are given in Table 1 along with effective radii measured at 1.65 μm by Gavazzi et al. (2000). The error on the estimate of the effective radii was estimated using a Monte Carlo approach. To the model galaxy, convolved with the IRS blue peak-up PSF, Gaussian noise was added at the level present in the real images. For 200 realizations of this noise, the FWHM was measured using the same procedure as for the real images. The distribution of these values (as a function of S/N) was used as an estimate of the error on the derived values of R_e.

A comparison between the *H*-band and 16 μm effective radii is shown in Fig. 2. Clearly, most galaxies in Coma are barely resolved by *Spitzer*-IRS, however, for those that are clearly resolved their effective radii are similar to those in the near-infrared. There is no evidence, for example, that the 16 μm emission is derived from an unresolved central source. Similar effective radii in the near-infrared and MIR are expected if the MIR emission is stellar in origin, such as found by Temi et al. (2008).

2.3 The mid-infrared colour–magnitude diagram

In Fig. 3, we show the MIR colour–magnitude diagram of the Coma cluster. The K_s-[16] colour is shown as measured within a fixed aperture of 12 arcsec.

The distribution of K_s-[16] colour shows a steady reddening from the faintest magnitudes observed ($K_s \sim -22$) to -24. In this magnitude range, the dispersion in K_s-[16] is close to a magnitude with values as high as 2.2 near $K_s \sim -24$. At brighter magnitudes, the colours show little variation and low dispersion with K_s-[16] $\simeq$ 1.3.

We also plot the position of four selected *passive* ETGs in the Virgo cluster, selected from the sample of Bressan et al. (2006). These galaxies have nuclear MIR spectra whose main characteristic is the presence of the silicate bump above 10 μm, indicating a passively evolving stellar population. These galaxies have also been observed in the IRS peak-up mode to secure a link between photometric and spectroscopic observations.

The presence of stellar population gradients within ETGs (Annibali et al. 2007), together with the existence of a general increase in the effective radius with the total magnitude of the galaxy, could, however, introduce a spurious effect, since a fixed aperture measurement would probe stellar populations in relatively more central regions for brighter galaxies.

To quantify this effect, we repeated the measurement within a fixed *relative* aperture of radius $\sim 2\ R_e$, where R_e is the effective radius of the galaxy. The results are shown in Fig. 4, though the lack of measured *H*-band effective radii introduces a cut at magnitudes fainter than $K_s \sim -23$. In this figure, the flattening at magnitudes brighter than $K_s \sim -24$ becomes more evident and actually the slope of the colour–magnitude relation is reversed for the brightest Coma galaxies, while there are only small differences at magnitudes fainter than $K_s \sim -24$.

The position of the four passive Virgo galaxies in Fig. 3 and that of the Coma galaxies brighter than $K_s \sim -24$ define a tight relation that can be extended down to the faintest magnitudes. By analogy with the optical/NIR colour–magnitude relations and because of the presence of the four Virgo ETGs, we argue that this line represents the MIR colour–magnitude relation of *passively evolving*, ETGs in the Coma cluster. ETGs significantly above this line have an 'excess' of 16 μm emission with respect to the passive sequence.

The presence of a population of galaxies which appear anomalously red in the MIR, colour–magnitude diagram is not mirrored in the optical/near-infrared, Fig. 5. The *V*–*K* colour shows a steady increase towards brighter magnitudes with a slight flattening for objects brighter than $K \sim -24$. This, in fact, is very similar to what we identify above as the *passive* colour–magnitude relation in the MIR. The implications of this difference are discussed further below.

[1] Calibration errors taken as 10 per cent, although the real calibration errors may be smaller.

[2] http://goldmine.mib.infn.it/, Gavazzi et al. (2003).

Table 1. The integrated 16 μm fluxes and sizes of the sample ETGs. The flux errors are the quadrature sum of a term due to the uncertainty in deriving the background sky level and a 5 per cent calibration uncertainty. The effective radii have been calculated by convolving a model $r^{1/4}$ de Vaucouleur's law with the IRS blue peak-up PSF (see the text).

Source ID	GMP83	RA (J2000)	Dec. (J2000)	Type	K_s (mag)	[4.5]–[16]	K_s-[16]	$R_e(H)$ (arcsec)	R_e (16 μm) (arcsec)
31	4928	$12^h57^m24^s.35$	$+27^\circ29'51''.8$	E/S0	9.20	–	1.27 ± 0.056	21.82	32.7 ± 12.2
49	1750	$13^h01^m53^s.75$	$+27^\circ37'27''.9$	E	–	–	1.19 ± 0.056	8.42	6.8 ± 2.9
67	3493	$12^h59^m24^s.93$	$+27^\circ44'19''.9$	S0	–	0.87 ± 0.118	0.95 ± 0.059	–	3.2 ± 1.9
68	3660	$12^h59^m13^s.49$	$+27^\circ46'28''.7$	S0	11.89	0.99 ± 0.117	1.07 ± 0.057	7.12	3.8 ± 2.2
69	3730	$12^h59^m08^s.00$	$+27^\circ47'02''.7$	E	11.09	1.19 ± 0.116	1.17 ± 0.056	6.28	4.7 ± 2.6
70	3739	$12^h59^m07^s.51$	$+27^\circ46'04''.1$	E	11.81	0.86 ± 0.117	0.90 ± 0.058	3.13	3.5 ± 2.1
71		$12^h58^m57^s.50$	$+27^\circ47'07''.5$	S0	12.98	0.43 ± 0.128	0.55 ± 0.082	–	2.3 ± 1.5
78	2000	$13^h01^m31^s.70$	$+27^\circ50'50''.2$	E	10.72	1.11 ± 0.116	1.10 ± 0.056	5.50	7.1 ± 3.6
79	2157	$13^h01^m17^s.50$	$+27^\circ48'33''.0$	S0	10.85	1.26 ± 0.116	1.32 ± 0.056	4.68	5.1 ± 2.6
84	2956	$13^h00^m05^s.30$	$+27^\circ48'26''.8$	S0	11.87	1.54 ± 0.117	1.61 ± 0.056	5.39	4.6 ± 2.7
87	3403	$12^h59^m30^s.64$	$+27^\circ47'29''.1$	E	12.51	0.16 ± 0.129	0.18 ± 0.083	–	1.7 ± 1.4
91	3997	$12^h58^m48^s.50$	$+27^\circ48'37''.3$	S0	11.12	1.29 ± 0.116	1.36 ± 0.056	5.06	4.3 ± 2.3
95		$13^h02^m52^s.73$	$+27^\circ51'59''.6$	S0	11.28	–	1.19 ± 0.056	4.41	3.4 ± 1.9
96		$13^h01^m50^s.22$	$+27^\circ53'36''.8$	E	11.37	1.82 ± 0.116	1.94 ± 0.056	3.62	1.0 ± 0.5
103	3400	$12^h59^m30^s.60$	$+27^\circ53'03''.2$	S0/a	11.10	1.73 ± 0.116	1.78 ± 0.056	3.96	2.9 ± 1.4
104	3296	$12^h59^m37^s.90$	$+27^\circ54'26''.1$	S0	11.57	1.37 ± 0.116	1.47 ± 0.056	3.12	5.3 ± 3.0
110	4626	$12^h57^m50^s.62$	$+27^\circ52'45''.8$	S0/E	12.48	0.39 ± 0.119	0.39 ± 0.062	–	2.3 ± 1.4
118	2541	$13^h00^m39^s.50$	$+27^\circ55'26''.5$	E	11.24	1.25 ± 0.116	1.32 ± 0.056	6.04	5.4 ± 3.0
124	3201	$12^h59^m44^s.30$	$+27^\circ54'44''.6$	E	11.34	1.40 ± 0.116	1.43 ± 0.056	4.11	3.2 ± 1.7
125	3222	$12^h59^m42^s.31$	$+27^\circ55'29''.1$	E	12.57	0.85 ± 0.120	0.92 ± 0.063	1.80	3.2 ± 1.9
126		$12^h59^m44^s.00$	$+27^\circ57'30''.3$	S0	12.69	0.71 ± 0.120	0.76 ± 0.064	–	5.5 ± 2.6
129	3329	$12^h59^m35^s.71$	$+27^\circ57'33''.8$	D	8.86	1.26 ± 0.116	1.29 ± 0.056	34.23	53.1 ± 21.0
132	3487	$12^h59^m25^s.31$	$+27^\circ58'04''.7$	S0	12.61	0.98 ± 0.118	1.09 ± 0.059	–	3.5 ± 2.1
133	3639	$12^h59^m15^s.00$	$+27^\circ58'14''.9$	E	11.00	1.87 ± 0.116	1.84 ± 0.056	3.37	2.4 ± 1.2
134		$12^h59^m03^s.85$	$+27^\circ57'32''.6$	E	13.13	0.92 ± 0.120	0.84 ± 0.065	–	2.2 ± 1.2
135	3851	$12^h58^m59^s.86$	$+27^\circ58'02''.6$	E	12.89	0.54 ± 0.122	0.90 ± 0.068	–	3.9 ± 1.8
136	3914	$12^h58^m55^s.30$	$+27^\circ57'52''.5$	E	12.52	0.73 ± 0.117	0.76 ± 0.059	–	2.0 ± 0.9
143	2390	$13^h00^m54^s.46$	$+28^\circ00'27''.3$	E	10.41	1.07 ± 0.116	1.10 ± 0.056	9.00	15.4 ± 7.6
144	2516	$13^h00^m42^s.76$	$+27^\circ58'16''.6$	S0/a	10.76	2.10 ± 0.116	2.17 ± 0.056	6.17	3.6 ± 1.6
145	2535	$13^h00^m40^s.70$	$+27^\circ59'47''.9$	S0	11.67	0.92 ± 0.118	0.99 ± 0.059	4.87	5.5 ± 3.2
148	2921	$13^h00^m08^s.13$	$+27^\circ58'37''.1$	D	8.41	1.28 ± 0.116	1.31 ± 0.056	13.57	23.7 ± 2.4
150	2940	$13^h00^m06^s.20$	$+28^\circ00'14''.7$	E	12.14	1.49 ± 0.116	1.62 ± 0.056	4.21	3.5 ± 2.1
152	3170	$12^h59^m46^s.79$	$+27^\circ58'26''.0$	SB0	11.57	1.18 ± 0.119	1.27 ± 0.063	6.34	6.6 ± 3.8
155	3367	$12^h59^m32^s.82$	$+27^\circ59'01''.2$	S0	11.25	1.66 ± 0.116	1.75 ± 0.056	5.18	3.1 ± 1.6
157	3484	$12^h59^m25^s.46$	$+27^\circ58'23''.7$	S0	12.45	1.26 ± 0.117	1.37 ± 0.058	–	10.9 ± 4.9
160	3761	$12^h59^m05^s.90$	$+27^\circ59'48''.2$	SB0	11.38	1.64 ± 0.117	1.77 ± 0.058	6.24	4.2 ± 2.3
164		$13^h03^m00^s.89$	$+28^\circ01'57''.2$	S0	10.31	–	1.22 ± 0.056	10.15	7.0 ± 3.1
167	2417	$13^h00^m51^s.57$	$+28^\circ02'34''.2$	S0/E	10.66	1.88 ± 0.116	1.94 ± 0.056	8.10	2.3 ± 1.0
168	2440	$13^h00^m48^s.67$	$+28^\circ05'26''.9$	E	10.90	1.58 ± 0.116	1.68 ± 0.056	3.96	3.3 ± 1.6
170	2727	$13^h00^m22^s.00$	$+28^\circ02'50''.1$	SB0	11.55	1.22 ± 0.117	1.34 ± 0.056	6.54	5.1 ± 2.9
171		$13^h00^m16^s.90$	$+28^\circ03'50''.0$	S0	12.40	0.74 ± 0.122	0.72 ± 0.069	–	3.6 ± 2.2
172	2839	$13^h00^m14^s.60$	$+28^\circ02'28''.6$	E	11.78	1.98 ± 0.116	2.06 ± 0.056	3.07	2.4 ± 1.2
174	2922	$13^h00^m07^s.80$	$+28^\circ04'42''.7$	E	11.59	1.66 ± 0.116	1.73 ± 0.056	2.56	2.7 ± 1.4
175	3073	$12^h59^m55^s.90$	$+28^\circ02'04''.9$	S0	11.16	1.52 ± 0.117	1.65 ± 0.057	4.98	6.9 ± 3.7
193	3084	$12^h59^m55^s.10$	$+28^\circ07'42''.2$	E	12.28	0.87 ± 0.117	0.92 ± 0.058	–	3.8 ± 2.3
194	3792	$12^h59^m03^s.79$	$+28^\circ07'25''.6$	E	10.29	1.13 ± 0.117	1.15 ± 0.057	6.81	6.9 ± 3.3
207	2912	$13^h00^m09^s.14$	$+28^\circ10'13''.6$	E	11.78	1.20 ± 0.118	1.32 ± 0.059	3.64	2.6 ± 1.5
217	3055	$12^h59^m57^s.60$	$+28^\circ14'50''.6$	E	10.39	1.23 ± 0.116	1.29 ± 0.056	7.47	8.2 ± 4.0
240	4822	$12^h57^m31^s.95$	$+28^\circ28'37''.0$	E	9.22	–	1.33 ± 0.056	14.13	11.6 ± 4.9
245		$12^h56^m56^s.58$	$+28^\circ37'24''.1$	S0	12.05	–	1.29 ± 0.057	–	3.2 ± 1.6

3 DISCUSSION

From an extrapolation of the NIR stellar photospheric continuum into the MIR Bressan et al. (2006) have estimated that the 16 μm emission in passive, ETGs has approximately equal contributions from stellar photospheres and dust emission. The most likely origin of the latter emission is from dusty circumstellar envelopes around evolved stars, such as the mass-losing AGB stars. The exact proportions depend on parameters such as the age and metallicity of the stellar population. Because the photospheric contribution shows little variation for a fixed *K*-band magnitude, the MIR colour–magnitude relation should depend strongly on the population of dusty AGB stars as a function of galaxy luminosity. In this scenario, those ETGs that show an excess of 16 μm emission have the largest luminosity-weighted dusty AGB population. The evolution of this stellar population should therefore

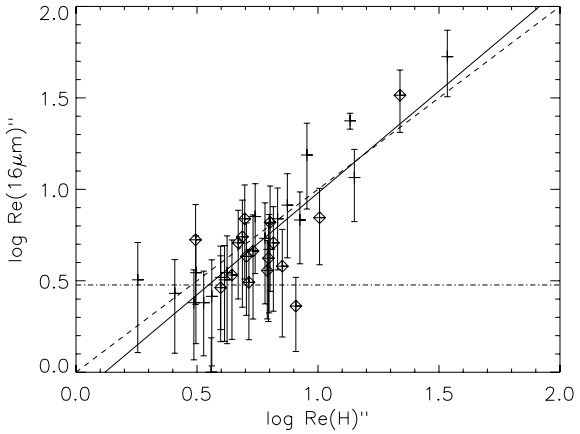

Figure 2. Relation between the effective *H*-band radii (1.65 μm, Gavazzi et al. 2000) and the 16 μm effective radii. The latter have been estimated by convolving a model $r^{1/4}$ de Vaucouleur's law with the IRS blue peak-up PSF (see the text). Crosses are ellipticals and diamonds are lenticulars (classified either as S0/E, S0, SB0 or S0/a). The solid line is a least-squares fit to the data whereas the dotted line corresponds to equal R_e at both wavelengths. The horizontal dot–dashed line corresponds to the radius containing half of the encircled energy for the IRS blue peak-up PSF.

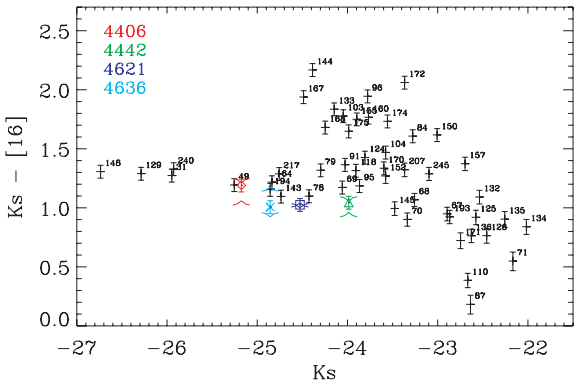

Figure 3. MIR colour–magnitude relation of the Coma cluster for fixed aperture K_s-[16] colours. Objects are identified according to their designations in Dressler (1980). The four ETGs in the Virgo cluster are shown with coloured symbols. For each of the Virgo galaxies, the MIR colours within the central 10 arcsec radius, as well as that of the whole galaxy *excluding* this central aperture are shown, as upward and downward pointing symbols, respectively. The assumed distance moduli to the Coma and Virgo clusters are 35.1 and 31.3, respectively.

be critical to the interpretation of the MIR colour–magnitude diagram.

Another possible origin of an excess of emission at 16 μm could be the contribution of a central AGN, as seen in the spectrum of NGC 4486 (Bressan et al. 2006). However, there is no evidence of broad emission lines in the available Sloan Digital Sky Survey (SDSS) spectra of those galaxies which lie well above the 'passive' colour–magnitude relation in Fig. 3. There is also no evidence that these galaxies have smaller effective radii at 16 μm (as shown by NGC 4486, that appears unresolved in the short–low (SL) and long–low (LL) IRS apertures).

3.1 Influence of the interstellar environment

Before considering the colour–magnitude relation in terms of stellar evolution, we first consider the influences that the interstellar

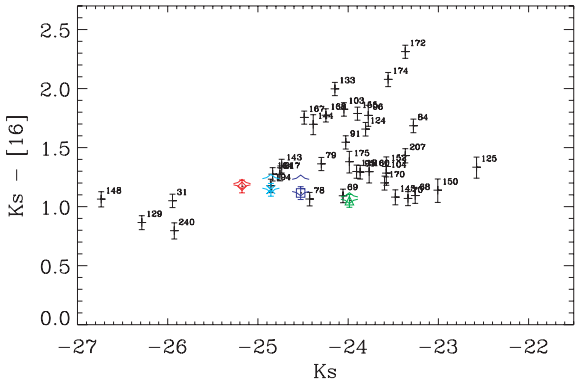

Figure 4. As Fig. 3 but for photometry with circular radii equal to $2R_e$, where R_e is the effective radius of the galaxy measured in the *H* band (Gavazzi et al. 2000). For the four Virgo galaxies, a radius of only R_e was used due to the limited size of the peak-up images.

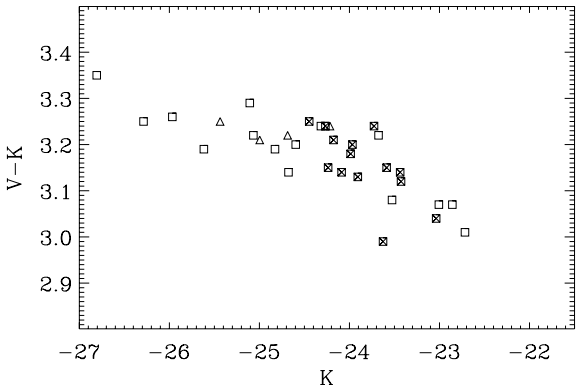

Figure 5. The optical/NIR colour–magnitude relation of the Coma cluster using the photometry of Bower et al. (1992). Coma ETGs are shown as squares whereas the passive ETGs in the Virgo cluster are shown as triangles. Galaxies with a K_s-[16] excess are indicated with a cross.

environment might have on the MIR colours. In nearby AGB stars, a significant fraction of the 16 μm flux originates from extended, dusty, circumstellar envelopes. It is thus important to understand how robust these envelopes are to different external perturbations, such as the ram pressure of the ISM in the central regions of massive ellipticals.

The circumstellar envelope of an AGB star expands at a typical velocity of $\sim$10 km s^{-1} which, at the condensation radius, $R_c \sim 10^{14}$ cm (Granato & Danese 1994; Bressan et al. 1998) is of the order of the escape velocity. The MIR emission, $f(\nu)$, in AGB stars, has a broad maximum between 10 and 20 μm suggesting a dust temperature $T_{dust} \sim 300$ K. Inspection of our dusty circumstellar models shows that dust reaches this temperature only in a thin internal region of the envelope, whose size is a few tens of R_c. At 10 km s^{-1}, the crossing time of this region is only 100 yr. Thus, the MIR emission from AGB stars is a short-lived phenomenon: after about 100 yr, dust is already so cool that its contribution in the MIR spectral region becomes negligible. However, in the central regions of an ETG, the star moves at the dispersion velocity through the tenuous ISM, and we need to determine whether or not the circumstellar envelope is able to maintain its structure in the inner few tens of R_c.

In order to estimate the radius at which the organized structure of the envelope is destroyed by its interaction with the ISM,

we equate the kinetic energy density in the circumstellar wind ($\sim 1/2 \rho_c v_\infty^2$) to the kinetic energy density of the ISM, due to the stellar dispersion velocity ($\sim 1/2\ \rho_I\ \sigma_g^2$).

Using a stationary wind, the circumstellar gas density is

$$\rho_c = \frac{\dot{M}}{4\pi r^2 v_\infty}, \quad (1)$$

while the ISM density is evaluated from the mass that has been already lost by stars

$$\rho_I = \frac{d^2 M}{dt\, dM_*} \times t \times \rho_* \simeq 10^{-12} \times t \times \rho_*. \quad (2)$$

In the second equation, $d^2M/dt dM_* \simeq 10^{-12}\ \mathrm{yr}^{-1}$ is the typical gas deposition rate per unit time and per unit stellar mass from the old stellar population. This is obtained from integration of the mass-loss rate along our isochrones of old stellar populations (see also Tinsley 1973). The average stellar density, ρ_*, is evaluated from deprojection of the De Vaucouleurs law (Young 1976) and depends on the assumed position within the galaxy.

Applying the condition of virial equilibrium and the observed relation between the total galaxy mass and the velocity dispersion (Cappellari et al. 2006), we find

$$r/r_c \simeq 200 \sqrt{\frac{\dot{M}_8 v_{10}}{L_3} \frac{1}{\sigma_3^{1.78} \rho_{01} t_{\mathrm{Gyr}}}}. \quad (3)$$

In this equation, r_c is the condensation radius, $\sim 1.66 \times 10^{12} \sqrt{L/\mathrm{L}_\odot}$, for a silicate dust mixture (for graphite, r_c is about half this value and r/r_c must be doubled); $\dot{M}_8$ is the stellar mass-loss rate in $10^{-8}\ \mathrm{M}_\odot/\mathrm{yr}$; v_{10} is the wind velocity in units of $10\ \mathrm{km\ s^{-1}}$; L_3 is the luminosity in units of $10^3\ \mathrm{L}_\odot$; σ_3 is the stellar velocity dispersion in units of $300\ \mathrm{km\ s^{-1}}$; r_e is the effective radius of the galaxy; ρ_{01} is the dimensionless average stellar density with respect to its value at $r/r_e = 0.1$ ($\rho_{01} = 10.5$, Young 1976); M_{12} is the galaxy mass in units of $10^{12}\ \mathrm{M}_\odot$ and t_{Gyr} is the time in Gyr.

Thus, only for very low mass-loss rates ($10^{-10}\ \mathrm{M}_\odot\ \mathrm{yr}^{-1}$) or in the very central regions of a galaxy – $\rho(r/r_e = 0.01) = 357$ – may the structure of the wind be destroyed at a few condensation radii. We may thus conclude that, in all relevant cases, the circumstellar wind is not destroyed by its interaction with the environment even in the cores of ETGs.

Once the circumstellar envelope mixes with the ISM, dust grains may be destroyed via sputtering by the hot ($\sim 10^7$ K) ISM gas. This process, however, will not affect the MIR emission, because, as discussed above, when the dust is released to the ISM it is already too cool to emit in the MIR spectral region. Furthermore, the time-scale for dust grain destruction via sputtering, even in the centre of the Coma cluster, is $\sim 10^8$ yr (Dwek, Rephaeli & Mather 1990), much larger than the lifetime of the newly formed hot dust within the circumstellar envelope (~ 100 yr).

In summary, we conclude that the MIR emission from dust grains in AGB stars is a short-lived phenomenon (~ 100 yr) happening in the inner, denser region of the circumstellar envelopes. This emission cannot easily be modified by interaction with the environment, so that the environment does not have a *direct* influence on the MIR colour–magnitude relation.

3.2 Stellar evolution

As it appears that the form of the MIR colour–magnitude relation is not influenced directly by some particular environmental effect, it must be explained via the properties of the underlying stellar populations.

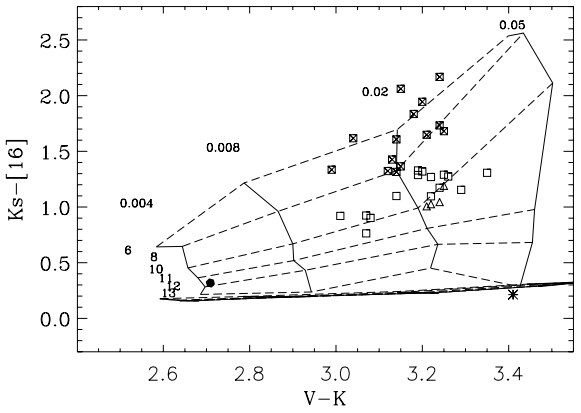

Figure 6. Optical NIR MIR colour–colour diagram. The horizontal axis is the $V - K$ colour from the precision photometry of Bower et al. (1992), while the vertical axis is the K_s-[16] colour measured within fixed apertures of 12 arcsec. Squares are Coma ETGs and triangles are the four selected passive ETGs in the Virgo cluster. Galaxies with a K_s-[16] excess are indicated with a cross. SSP models for the indicated ages and metallicity are computed following the scheme of Bressan et al. (1998). Models without dusty AGB envelopes collapse to the almost horizontal dashed lines at the bottom of the diagram. The dotted line represents the locus of the Kurucz model atmosphere with low metallicity (the effect of metallicity is very small however) and the asterisk is a COMARCS low-temperature atmosphere model as calculated by Aringer et al. (in preparation). The position of the globular cluster, 47-Tuc, is indicated by the solid hexagon in the lower left-hand side.

In Fig. 6, we compare our observations with the predictions for the integrated colours of simple stellar populations (SSPs).

As discussed in Bressan et al. (1998), both the integrated optical and MIR colours of SSPs suffer from the degeneracy between age and metallicity, but in the opposite sense. While optical features (colours or narrow-band indices) of the same strength can be obtained by an *anticorrelated* variation of age and metallicity, producing the typical banana-shaped solutions in the age–metallicity diagrams (Annibali et al. 2007), an equal intensity of the 10 μm bump may be obtained by a *correlated* variation of the age and metallicity.

For this reason, the effects of age and metallicity variations are best separated in a mixed optical-NIR-MIR colour–colour plot, such as that in Fig. 6.

In Fig. 6, the horizontal axis is the $V - K$ colour obtained from the precision photometry of Bower, Lucey & Ellis (1992), while the vertical axis is our measured K_s-[16] colour. The K-band magnitudes on the two axes therefore refer to slightly different central filter wavelengths and apertures.[3] Though the $V - K$ colours of Bower, Lucey & Ellis are provided only for a subsample of our galaxies (30 out of 50 objects), we prefer to use their values to preserve the homogeneity of the data. Squares are the Coma ETGs while the triangles refer to the four Virgo galaxies.

New SSP models, for the indicated age and metallicity, have been computed following the scheme of Bressan et al. (1998). The only difference with respect to these previous models is a minor

[3] The photometry of Bower, Lucey & Ellis was measured in an aperture of radius 8.5 arcsec and corrected to a radius of 5.5 arcsec. The aperture correction applied was 0.03 mag for $V - K$. Assuming a correction of similar magnitude would be required to correct to our radius of 12 arcsec, the $V - K$ values should shift by −0.03 mag. This would not alter any of our interpretation.

revision of the mass-loss rate during the AGB phase, introduced by the calibration with new $V - K$ integrated colours of populous star clusters in the Large Magellanic Cloud, and the adoption of the new empirical library of stellar spectra (Sánchez-Blázquez et al. 2006b).

A few caveats concerning models should be kept in mind because they are relevant to the present investigation.

First of all, it is worth recalling that in Bressan et al. (1998) the effects of possible circumstellar dust in the red giant branch (RGB) phase (i.e. before central helium burning in the horizontal branch in the case of old populations) have not been considered. Recent claims, that RGB stars also show a significant MIR excess not dependent on their luminosity (Origlia et al. 2007), should be regarded with great care because of possible strong crowding effects (Boyer et al. 2008).

Furthermore, old stellar populations in the galaxies we are considering could reach supersolar metallicity and, as such, may not be well represented by those in our own galaxy. Very little is actually known on the efficiency of the mass-loss rate at high metallicity (Carraro et al. 1996). However, van Loon, Boyer & McDonald (2008) do not find evidence of a MIR excess in the RGB stars of NGC 6791, a super metal-rich globular cluster. Also, NGC 4649 and NGC 1399, the two ETGs with the largest ultraviolet upturn and high Mg2 index (Bertola et al. 1995), that have been interpreted as the signature of very metal-rich stars (Bressan, Chiosi & Fagotto 1994), have *Spitzer*-IRS spectra similar to those observed in our passive Virgo ETGs (Bressan et al., in preparation). Thus, there seems to be no evidence that metallicity has a direct effect on mass loss.

As already anticipated, variations of age and metallicity are very well separated in this colour–colour diagram, especially at high metallicity, with iso-metallicity lines being almost horizontal and coeval SSPs moving on almost vertical lines. In contrast, models without dusty AGB envelopes collapse to the almost horizontal dashed lines at the bottom of the diagram, independent of their ages. The effects of dust disappear at ages larger than 13 Gyr, where the AGB phase is practically absent.

We have extended the photospheric stellar spectra of MILES (Sánchez-Blázquez et al. 2006b) in the NIR/MIR region by means of matched NEXTGEN models (Hauschildt et al. 1999). In addition, the effects of dusty envelopes have been included following the prescriptions described in Bressan et al. (1998). Thus, the bottom horizontal dashed lines (models without dusty AGB envelopes) superimpose on single NEXTGEN spectra at varying effective temperature. The effect of varying the metallicity is almost negligible in the K_s-[16] colour. To illustrate the difference introduced by adopting different stellar spectra, we have marked with an asterisk the position of a COMARCS low-temperature atmosphere model as calculated by Aringer et al. (in preparation). Finally, the hexagon towards the bottom left-hand side of the diagram (age $\sim$12 Gyr and $Z \sim 0.004$) marks the position of the globular cluster 47 Tuc whose semi-empirical integrated colours have been derived by Bressan et al. (2006).

Fig. 6 shows that galaxies that follow the MIR colour–magnitude relation are almost coeval, with an age of about 10 Gyr and a metallicity that grows by a factor of about 2. It is interesting to note that the four Virgo galaxies are as old as the oldest Coma galaxies. None of the galaxies appear to be as old as the globular cluster 47 Tuc.

Galaxies with a K_s-[16] excess, cluster around the lines of 8 and 6 Gyr thus appearing younger by about 2–4 Gyr.

In order to clarify the different sensitivity to stellar populations of optical and MIR colours, we have reproduced, in Fig. 5, the optical/NIR colour–magnitude relation for the galaxies shown in Fig. 6. Galaxies with a K_s-[16] excess (i.e. clustering around and above 8 Gyr in Fig. 6) are plotted with a cross. Fig. 5 shows that in spite of a well-detected K_s-[16] excess, the latter galaxies lie on the optical/NIR colour–magnitude relation. Moreover, a significant fraction of these galaxies are classified as ellipticals.

3.3 Indirect influence of cluster environment on the K_s-[16] colour?

The fraction of galaxies showing a K_s-[16] colour excess with respect to the oldest systems, in Fig. 6, is about 48 per cent. If we consider the total sample (Fig. 3) and add four more galaxies with a clear K_s-[16] excess with respect to the colour–magnitude relation, the fraction is 32 ± 8 per cent.

A possible interpretation, discussed in the previous section, is that these systems have average younger ages, since a younger stellar population is expected to have a redder MIR emission by virtue of the larger fraction of dusty AGB stars. However, galaxies are complex systems that may not be well represented by simple stellar populations and caution must be used in the interpretation of the K_s-[16] colour excess. It does not necessarily point to a younger global age of a passively evolving system.

For example, in the case of the Virgo ETG, NGC 4435, Panuzzo et al. (2007) have shown that the MIR emission is dominated by a nuclear starburst which is practically invisible in the optical and NIR. Its IRS low-resolution spectra are dominated by polycyclic aromatic hydrocarbon (PAH), atomic and molecular emission features that are typical of star-forming galaxies. At 16 μm, the emission is not resolved, indicating that the emission arises from the nucleus; which indeed appears as a dusty disc in *Hubble Space Telescope* (*HST*) images. In this rejuvenation episode (about 200 Myr ago), less than 1 per cent of the total galaxy mass was formed. From Panuzzo et al. (2007), we estimate, for NGC 4435, a K_s-[16] colour $\simeq 2.8$ mag in the central 5 arcsec radius aperture, and a total K_s-[16] colour $\simeq 2.1$ mag and total $V - K \simeq 3.1$. In Fig. 6, the latter values would put NGC 4435 in the region around 6 Myr and $Z = 0.02$. Indeed, NGC 4435 was selected for IRS observations as one of the galaxies that make up the Virgo colour–magnitude relation. From the analysis of this sample (18 galaxies), Bressan et al. (2006) concluded that the fraction of ETGs that show signatures of recent activity is 17 per cent. This figure is significantly lower than the fraction of Coma ETGs with a K_s-[16] colour excess.

We have also extracted, from Data Release 6 (DR6) of the SDSS, the available spectra (16 out of 50) of our Coma galaxy sample. In Fig. 7, we show the 3700–4200 Å spectral region, around the Ca II lines. Galaxies are sorted by decreasing brightness and green curves represent objects with a K_s-[16] colour excess. In three objects (D103, D118 and D155) with a K_s-[16] excess, the Ca II H line is as deep as the K line, indicating contamination by A type stars, i.e. a recent rejuvenation episode. In the other galaxies the Ca II doublet appears normal. We recall, that for solar metallicity, an inversion of the Ca II doublet starts appearing only at ages younger than 2 Gyr (Longhetti et al. 1999).

Although we see in Fig. 8 that the K_s-[16] colour is uncorrelated with the position in the cluster, we note that if we identify those galaxies with an 'excess' of 16 μm emission as those with $K_s - [16] > 1.5$ (see Fig. 3) then the mean projected distance from the cluster centre of this population is smaller than for those galaxies with K_s-[16] < 1.5. The mean projected distance from the cluster centre for the 16 μm excess galaxies is $0.^{\circ}17$ whereas that for the others is $0.^{\circ}32$ (the Kolmogorov–Smirnov probability that the two distributions are the same is 1.6 per cent). Because it seems that the

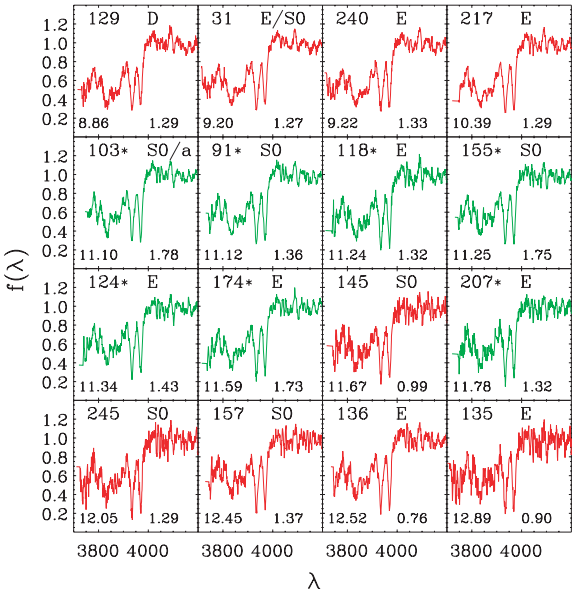

Figure 7. Optical SDSS spectra of selected Coma cluster galaxies. Galaxies with a K_s-[16] excess are shown in green and indicated with an asterisk.

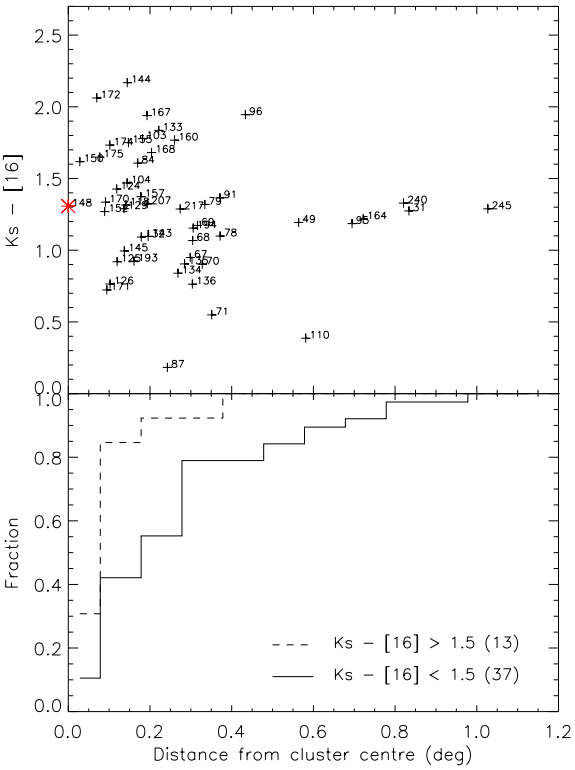

Figure 8. K_s-[16] colour as a function of the projected distance from the cluster centre, defined as the CD galaxy D148 (asterisk on y-axis). The bottom panel shows the cumulative distribution for ETGs with $K_s - [16] > 1.5$ and $K_s - [16] < 1.5$. The number of objects in each subset is indicated in parentheses.

cluster environment does not directly influence the MIR colour–magnitude diagram, this suggests that the star formation history has been modified by the environment; which, in turn, influences the galaxy colours. The sense of this influence is that galaxies with redder K_s-[16] colour (younger luminosity-weighted stellar ages, Fig. 6) are preferentially found at small cluster-centric radii.

Miller & Owen (2002) have investigated the distribution of both AGN and star-forming galaxies as a function of cluster-centric distance. They find that dusty star-forming galaxies have a more centrally concentrated distribution than normal star-forming galaxies, with AGN being more centrally concentrated than both. Though there is no evidence of emission lines in the SDSS spectra, we cannot exclude that the MIR excess is due to an obscured nuclear starburst like that found in NGC 4435. A possible way to check this possibility is by means of existing IRAC 4.5 and 8 μm observations (sampling the strength of the 7.7 PAH feature) and MIPS 24 μm (sampling the presence of hot dust). This work is underway.

3.4 Implications

The MIR colour–magnitude relation indicates that the oldest Coma ETGs define a sequence of increasing metallicity at constant age ($Z \simeq 0.01$– 0.03, $t \simeq 10$ Gyr).

While this conclusion has already been suggested by the analysis of the optical/NIR colour–magnitude relation, it is only with the use of the complementary MIR observations that the alternative solution (invoking a synchronization of the epoch of formation with total brightness, see Bower et al. 1992) can be excluded.

Indeed, our analysis of the mixed optical-NIR-MIR colour–colour diagram clearly shows that some of the galaxies that populate the optical colour–magnitude relation may have average ages that are even 40 per cent younger than the old sequence. In those galaxies, however, a larger metallicity may redden the colours and compensate for the younger age in an optical diagram. This illustrates the importance of the MIR colour in breaking the age–metallicity degeneracy.

Our conclusion is in a very good agreement with the analysis of narrow-band indices of ∼4000 ETGs carefully selected from the SDSS (Clemens et al. 2006) and recently extended to ∼14 000 objects with the DR6 catalogue (Clemens et al., 2009). These authors find that the luminosity-weighted ages of the whole sample start young at a low-velocity dispersion, rise until $\log \sigma \sim 2.32$ and flatten at larger σ. In contrast, the metallicity shows a continuous increase with increasing σ.

Our result, that a large fraction of ETGs in Coma populate a genuine old and coeval sequence, contrasts somewhat with the recent study of ETGs in the Coma cluster by Trager et al. (2008). Based on optical spectra these authors also find that, in spite of a wide range in mass, 10/12 objects are consistent with the hypothesis of a coeval population. However, the age they find for this population, 5.2 ± 0.2 Gyr, is significantly younger than our value.

We note that this discrepancy is unlikely to be caused by a significant offset between ages derived with the two methods. Indeed, there are four objects in common, for which Trager et al. find the following ages: D129 (GMP3329) 7.9 Gyr, D157 (GMP3484) 7.8 Gyr, D155 (GMP3367) 4.5 Gyr and D133 (GMP3639) 3 Gyr.

D129 and D157, the two old objects, fall on our MIR colour–magnitude relation, for which we derive only slightly older ages. On the other hand, D155 and D133, the two young objects, lie well above this relation and, given their K_s-[16] colour we would conclude that they are possibly affected by some rejuvenation episode.

Considering that, contrary to our analysis, optical studies are affected by the age–metallicity degeneracy causing (large) uncertainties that are difficult to quantify, we believe that there is a good agreement for the few objects in common.

It is more difficult to explain why we find that 68 per cent of the galaxies in our sample populate the old sequence, while Trager et al. find that only 25 per cent are old. If their sample is not biased towards young objects and given the sensitivity of the K_s-[16] colour to rejuvenation events, we suspect that the age–metallicity degeneracy is still to blame.

Bregman, Temi & Bregman (2006) find a very similar discrepancy between the age of ETGs determined by optical line indices and MIR *Spitzer* spectra that include the silicate emission feature near 10 μm. They also find mean ages of ∼10 Gyr using MIR data.

It is also interesting to note that the upper 2.5 mag of the MIR colour–magnitude relation is quite narrow. On the contrary, in the lower 2.5 mag, below $M_K \sim -24.5$, there is a significant dispersion. This shows that the rejuvenation events (of any kind) have not affected the most massive ETGs.

4 CONCLUSIONS

We present 16 μm, *Spitzer*-IRS, blue peak-up images of a sample of 50 ETGs in the Coma cluster. We compare these with archival IRAC images at 4.5 μm and 2MASS, K_s band images at 2.2 μm.

We make the following conclusions.

(i) Our IRS blue peak-up images show no evidence that the 16 μm emission is anything other than stellar in origin.

(ii) The region within a dusty AGB star envelope where dust is hot enough to emit strongly at 16 μm is not vulnerable to environmental effects such as the ram pressure of an ISM wind or dust sputtering by hot gas. Dust grains only spend ∼100 yr near ∼300 K and this region is sufficiently dense to survive against ram pressure disruption.

(iii) We identify the MIR colour–magnitude relation of passively evolving ETGs as the lower envelope of the galaxy distribution in the K_s-[16] versus K_s plane; that is, the minimum value of K_s-[16] at a given K_s magnitude. ∼68 per cent of the galaxies in our sample lie on this colour–magnitude relation. These galaxies cannot have had any episode of star formation accounting for more than ∼1 per cent of the total stellar mass within the last few Gyr. These are genuinely 'passively evolving' objects. The remaining objects are either significantly younger than 10 Gyr or have undergone a rejuvenation event in the recent past. This result is at odds with the most recent estimate of the fraction of old objects based on optical spectroscopy (Trager et al. 2008).

(iv) We construct the mixed optical-NIR-MIR two colour diagram and, by means of updated simple stellar population models, we show that the addition of MIR data allows a much better separation of the effects of age and metallicity, which are rather degenerate either in the optical or MIR when taken in isolation. In this plane, galaxies populating the colour–magnitude relation trace a sequence of *varying metallicity at approximately constant age*. Although this conclusion was already consistent with the optical-NIR colour–magnitude relation, a correlation between age and metallicity could equally well explain the relation. Indeed, comparison with the optical-NIR colours shows that *a number of galaxies that lie on the optical–NIR relation are significantly displaced from the MIR relation*, with redder K_s-[16] colours. The MIR colour–magnitude diagram therefore shows a sequence of metallicity for old, passive galaxies, with younger objects displaced towards redder K_s-[16] colours.

(v) The oldest elliptical galaxies in our sample have luminosity-weighted, mean stellar ages of 10.5 Gyr and metallicities within a factor of 2 of the solar value. No galaxy in our sample is as old or metal poor as the globular cluster 47 Tuc.

(vi) Although the addition of the K_s-[16] colour allows us to identify objects with significantly younger, luminosity-weighted, mean stellar ages, we cannot distinguish between genuinely 'young' objects and those that have undergone a minor rejuvenation event. However, given that even a period of recent (last few Gyr) star formation that accounts for less than 1 per cent of the total stellar mass will shift a galaxy off the MIR colour–magnitude relation, the latter option seems far more likely. Unambiguous resolution of this issue will require the infrared spectroscopic capabilities of future space observatories.

(vii) There is evidence that those galaxies that have an excess in the K_s-[16] colour are found preferentially at smaller cluster-centric radii. As the interaction between the dusty AGB star envelopes and the ISM does not directly effect the 16 μm emission, the excess may be caused by 'rejuvenation' episodes induced by the cluster environment.

ACKNOWLEDGMENTS

We acknowledge a financial contribution from contract ASI-COFIS I/016/07/0.

This work is based on observations made with the *Spitzer Space Telescope*, which is operated by the JPL, Caltech under a contract with NASA.

We make use of data products from the Two-Micron All-Sky Survey, which is a joint project of the University of Massachusetts and the Infrared Processing and Analysis Center/California Institute of Technology, funded by the National Aeronautics and Space Administration and the National Science Foundation.

This research has made use of the GOLD Mine Data base.

Funding for the SDSS and SDSS-II has been provided by the Alfred P. Sloan Foundation, the Participating Institutions, the National Science Foundation, the US Department of Energy, the National Aeronautics and Space Administration, the Japanese Monbukagakusho, the Max Planck Society and the Higher Education Funding Council for England. The SDSS Web Site is http://www.sdss.org/.

The SDSS is managed by the Astrophysical Research Consortium for the Participating Institutions. The Participating Institutions are the American Museum of Natural History, Astrophysical Institute Potsdam, University of Basel, University of Cambridge, Case Western Reserve University, University of Chicago, Drexel University, Fermilab, the Institute for Advanced Study, the Japan Participation Group, Johns Hopkins University, the Joint Institute for Nuclear Astrophysics, the Kavli Institute for Particle Astrophysics and Cosmology, the Korean Scientist Group, the Chinese Academy of Sciences (LAMOST), Los Alamos National Laboratory, the Max-Planck-Institute for Astronomy (MPIA), the Max-Planck-Institute for Astrophysics (MPA), New Mexico State University, Ohio State University, University of Pittsburgh, University of Portsmouth, Princeton University, the United States Naval Observatory and the University of Washington.

We thank P. Marigo, L. Girardi and A. Renzini for useful discussions.

REFERENCES

Annibali F., Bressan A., Rampazzo R., Zeilinger W. W., Danese L., 2007, A&A, 463, 455

Athey A., Bregman J., Bregman J., Temi P., Sauvage M., 2002, ApJ, 571, 272

Bernardi M., Sheth R. K., Nichol R. C., Schneider D. P., Brinkmann J., 2005, AJ, 129, 61

Bertola F., Bressan A., Burstein D., Buson L. M., Chiosi C., di Serego Alighieri S., 1995, ApJ, 438, 680
Bower R. G., Lucey J. R., Ellis R. S., 1992, MNRAS, 254, 589
Boyer M. L., McDonald I., van Loon J. T., Woodward C. E., Gehrz R. D., Evans A., Dupree A. K., 2008, AJ, 135, 1395
Bregman J. N., Temi P., Bregman J. D., 2006, ApJ, 647, 265
Bressan A., Chiosi C., Fagotto F., 1994, ApJS, 94, 63
Bressan A., Granato G.-L., Silva L., 1998, A&A, 332, 135
Bressan A. et al., 2006, ApJ, 639, L55
Cappellari M. et al., 2006, MNRAS, 366, 1126
Carraro G., Girardi L., Bressan A., Chiosi C., 1996, A&A, 305, 849
Clemens M. S., Bressan A., Nikolic B., Alexander P., Annibali F., Rampazzo R., 2006, MNRAS, 370, 702
Clemens M. S., Bressan A., Nikolic B., Rampazzo R., 2009, MNRAS, 392, L35
Dressler A., 1980, ApJS, 42, 565
Dwek E., Rephaeli Y., Mather J. C., 1990, ApJ, 350, 104
Gavazzi G., Franzetti P., Scodeggio M., Boselli A., Pierini D., 2000, A&A, 361, 863
Gavazzi G., Boselli A., Donati A., Franzetti P., Scodeggio M., 2003, A&A, 400, 451
Gledhill T. M., Yates J. A., 2003, MNRAS, 343, 880
Granato G. L., Danese L., 1994, MNRAS, 268, 235
Hauschildt P. H., Allard F., Ferguson J., Baron E., Alexander D. R., 1999, ApJ, 525, 871
Landsman W. B., 1995, in Shaw R. A., Payne H. E., Hayes J. J. E., eds, ASP Conf. Ser. Vol. 77, Astronomical Data Analysis Software and Systems IV. Astron. Soc. Pac., San Francisco, p. 437
Lebzelter T., Posch T., Hinkle K., Wood P. R., Bouwman J., 2006, ApJ, 653, L145
Leeuw L. L., Sansom A. E., Robson E. I., Haas M., Kuno N., 2004, ApJ, 612, 837
Longhetti M., Bressan A., Chiosi C., Rampazzo R., 1999, A&A, 345, 419
Marleau F. R. et al., 2006, ApJ, 646, 929
Miller N. A., Owen F. N., 2002, AJ, 124, 2453
Origlia L., Rood R. T., Fabbri S., Ferraro F. R., Fusi Pecci F., Rich R. M., 2007, ApJ, 667, L85
Panuzzo P. et al., 2007, ApJ, 656, 206
Renzini A., 2006, ARA&A, 44, 141
Sánchez-Blázquez P., Gorgas J., Cardiel N., González J. J., 2006a, A&A, 457, 809
Sánchez-Blázquez P. et al., 2006b, MNRAS, 371, 703
Temi P., Brighenti F., Mathews W. G., 2007, ApJ, 660, 1215
Temi P., Brighenti F., Mathews W. G., 2008, ApJ, 672, 244
Thomas D., Maraston C., Bender R., Mendes de Oliveira C., 2005, ApJ, 621, 673
Tinsley B. M., 1973, ApJ, 186, 35
Trager S. C., Faber S. M., Dressler A., 2008, MNRAS, 386, 715
van Loon J. T., Boyer M. L., McDonald I., 2008, ApJ, 680, L49
Young P. J., 1976, AJ, 81, 807

This paper has been typeset from a TEX/LATEX file prepared by the author.